Efficiency Improvement of Electro-optical Modulator on Thin Film Lithium Niobate with Off-axis Waveguide Orientation

1st Yuan Shen
Research Center for Optical Fiber Sensing
Zhejiang Laboratory
Hangzhou, China
sheny@zhejianglab.com

2nd Bigeng Chen*
Research Center for Optical Fiber Sensing
Zhejiang Laboratory
Hangzhou, China
chenbg@zhejianglab.com

3rd Renyou Ge
Research Center for Optical Fiber Sensing
Zhejiang Laboratory
Hangzhou, China

4th Yunjiang Rao
Fiber Optics Research Center, Key Lab of Optical Fiber Sensing and Communications
University of Electronic, Science and Technology of China
Chengdu, China
Research Center for Optical Fiber Sensing
Zhejiang Laboratory
Hangzhou China

***Abstract*—The modulation efficiency of electro-optical modulator (EOM) on thin film lithium niobate (TFLN) with arbitrary waveguide orientation with respect to the crystal axes is calculated theoretically and numerically. Compared with the conventional Y-propagation phase shifter direction on X-cut substrate, modulation efficiency can be further improved when rotating the phase shifters by certain angles within the Y-Z plane. Improvements of about 20-40% are achieved in simulation with three typical TFLN waveguide-electrode configurations.**

Keywords—thin film lithium niobate, electro-optic modulator, dielectric anisotropy

I. Introduction

Electro-optical modulator (EOM) is one of the key devices in opto-electronic information technologies ranging from optical communication, microwave photonics to quantum information processing [1, 2]. The successful wafer-scale manufacturing and micro/nano processing of thin film lithium niobate (TFLN) have promoted EOMs based on TFLN as high-performance integrated modulators ready for practical applications [3]. COMS-compatible driving voltage and high compactness become feasible benefitting from a series of advantages such as pure phase modulation, low waveguide loss, high field confinement, etc. Conventional EOMs on TFLN usually exploit the r_{33} electro-optic (EO) coefficient (~30.9 pm/V) with TE-polarized optical mode and the driving electric field along the crystal axis Z. As a result, the optical wave being modulated usually propagates along the Y axis, which limits the circuiting flexibility and further improvement of the fundamental efficiency. On the other hand, a less utilized coefficient r_{42} (~32.6 pm/V) as pronounced as r_{33} could provide an opportunity for off-axis waveguiding structures and potential efficiency improvement.

In this work, comprehensive theoretical analysis and numerical calculation are performed to investigate the EO efficiency of TE-polarized guided optical wave on TFLN, with arbitrary rotation between the waveguide and the crystal axis. It is found that the efficiency is maximized when the angle of the waveguide on X-cut TFLN and the Z axis is 47.8° with ideal uniform electric field. Finite-element simulation results in three typical cases of TFLN waveguide-electrode configurations show that the EO efficiency can be improved by 30.9%, 41.4% and 23.3%, respectively.

II. Theorical Analysis

The linear EO effect of lithium niobate (LN) can be described by a Pockels tensor with permittivity (square of refractive index) perturbations related to external DC/RF field. The perturbation is expressed as $\Delta\varepsilon_{ij} = -\sum_k \varepsilon_{ii}\varepsilon_{jj} r_{ijk} E_k/\varepsilon_0$. The inverse permittivity tensor perturbation can thus be written as $\Delta\left(\frac{1}{n^2}\right)_{ij} \cong \sum_k r_{ijk} E_k$. The subscripts i and j (1, 2 or 3) represents the crystal axes X, Y and Z (upper case). The tensor matrix of LN with trigonal crystal system is [4]

$$r_{Ik} = \begin{bmatrix} 0 & -r_{22} & r_{13} \\ 0 & r_{22} & r_{13} \\ 0 & 0 & r_{33} \\ 0 & r_{42} & 0 \\ r_{42} & 0 & 0 \\ -r_{22} & 0 & 0 \end{bmatrix} \text{ with } I = \begin{cases} 1 & \text{for } ij = 11 \\ 2 & \text{for } ij = 22 \\ 3 & \text{for } ij = 33 \\ 4 & \text{for } ij = 23 \text{ or } 32 \\ 5 & \text{for } ij = 13 \text{ or } 31 \\ 6 & \text{for } ij = 12 \text{ or } 21 \end{cases} \quad (1)$$

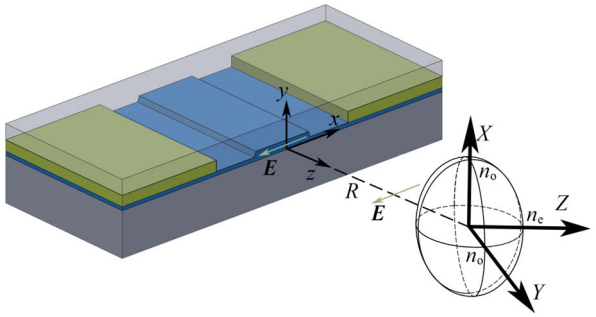

Fig. 1. Illustration of a TFLN waveguide and the refractive index ellipsoid of the crystal. A rotation matrix R can be used to describe the relation between the static coordinate system xyz of waveguide and the ordinate system XYZ of TFLN.

The values of $[r_{13}, r_{22}, r_{33}, r_{42}]$ are taken as 9.6, 6.8, 30.9 and 32.6 pm/V [5], respectively. In a waveguide within static Cartesian coordinate system (xyz, lower case) shown in Fig. 1, the quasi-TE modes mainly observe the refractive index in the horizonal direction (axis x) normal to their propagation direction, while the quasi-TM modes observe the refractive index in the vertical direction (axis y).

When the normal direction of the crystal substrate and the orientation of waveguide are both arbitrary, a three-dimension rotation matrix R can be used to describe the mapping from the waveguide coordinate system xyz to the crystal coordinate system XYZ. The matrix R is characterized by $XY'Z''$ -intrinsic-rotation Tait–Bryan angles α, β and γ as illustrated in fig. 2(a). In detail, initially being coincident with the waveguide coordinate system, the crystal coordinate system firstly rotates around the X axis by α, then around the Y axis by β and finally around the Z axis by γ. Hence, R is denoted as:

$$R = \begin{bmatrix} 1 & 0 & 0 \\ 0 & \cos\alpha & -\sin\alpha \\ 0 & \sin\alpha & \cos\alpha \end{bmatrix} \begin{bmatrix} \cos\beta & 0 & \sin\beta \\ 0 & 1 & 0 \\ -\sin\beta & 0 & \cos\beta \end{bmatrix} \begin{bmatrix} \cos\gamma & -\sin\gamma & 0 \\ \sin\gamma & \cos\gamma & 0 \\ 0 & 0 & 1 \end{bmatrix} \quad (2)$$

A uniform electric field E perpendicularly crossing the waveguide yields $[-E, 0, 0]^T$ in xyz coordinate system and produces an inverse permittivity perturbation with the Pockels effect described as

$$p_I = \Delta\left(\frac{1}{n^2}\right)_I \cong r_{Ik} \cdot R^{-1} \cdot [-E, 0, 0]^T \quad (3)$$

in XYZ coordinate system. Therefore, the deformed refractive index ellipsoid in xyz coordinate system satisfies equation (4) in combination with the rotation:

$$[n_x, n_y, n_z] \cdot R \cdot \begin{bmatrix} \frac{1}{n_o^2} + p_1 & p_6 & p_5 \\ p_6 & \frac{1}{n_o^2} + p_2 & p_4 \\ p_5 & p_4 & \frac{1}{n_e^2} + p_3 \end{bmatrix} \cdot R^{-1} \cdot [n_x, n_y, n_z]^T = 1 \quad (4)$$

Solving the equation above with $n_y = n_z = 0$, the refractive index for the TE-polarized plane wave can be calculated, which equals n_x in this case. Similarly, the refractive index for the TM-polarized plane wave can be obtained as well by setting $n_x = n_z = 0$.

By setting the electric intensity as 0 or 1×10^{-7} V/pm (i.e., voltage drops by 1 V in a spatial distance of 10 μm), we can calculate the refractive index differences Δn of the TE-polarized plane wave induced by external uniform electric field. Fig. 2(b) gives an example of Δn versus α and β at $\gamma = 30°$, which shows that the angle α does not affect Δn. In fact, according to the nature of the coordinate rotation, a varying α with certain β and γ means that the crystal coordinate XYZ rotates about the x axis. Mathematically, the rotation axis keeps unchanged about the rotation, so the refractive index for the TE polarization in the x direction is unaffected by the rotation about x axis. A surface plot of Δn versus β and γ is obtained as shown in fig. 2(c), with its projection on the β-γ plane below. The conventionally employed EOM orientation on TFLN is at the point of $[\beta = 90°, \gamma = 90°]$ (red cross marked on the planar projection), which is in a valley along the γ direction. It means that when β deviates from 90°, the EO efficiency could be further improved. Six Δn_{max} points can be found in coordinates of $[\beta = 137.8°, \gamma = 90° + 120° \cdot a$ and $[\beta = 42.2°, \gamma = 30° + 120° \cdot a]$ $(a = 1,2,3)$ marked as red cycles in fig. 2(c). These points belong to three rotation groups as $R(\alpha, \beta, \gamma) = R(\alpha + \pi, \pi - \beta, \gamma + \pi)$. Because of the trigonal crystal system of LN, the Z axis supports a three-fold rotation and the physical property remains unchanged when the system rotates by 120° or 240° around the Z axis. Δn is maximized at the angle of 47.8° between the x and Z axes. In addition, the antisymmetric property along β of Δn suggests that push-pull modulation is still feasible to double the efficiency in an off-axis EOM. However, Δn is asymmetrical about $\beta = 0°$ and $\beta = 90°$, which may be attributed to the directionality of the crystal axes [4].

The rotation angles of $[\alpha = 0°, \gamma = 90°]$ (red dashed line marked in fig. 2(c)) corresponds to an X-cut TFLN mostly applied for EOMs nowadays, thus β becomes the angle between the Z and z axes, the latter of which represents the waveguide direction. Figs. 3(a) and 3(b) show the calculated refractive indices and field-induced index differences for both the TE- and TM-polarized waves on X-cut TFLN. The anisotropy results in a refractive index varying for the TE wave, while the TM wave has an index independent of β (fig. 3(a)). As shown fig. 3(b), Δn for TE wave increases obviously when the waveguide deviates from the conventional Y direction ($\beta = 90°$) for a certain range. The improvement is up to 35.4% at 137.8°. For the TM wave, the EO efficiency is much smaller but is angle-dependent as well.

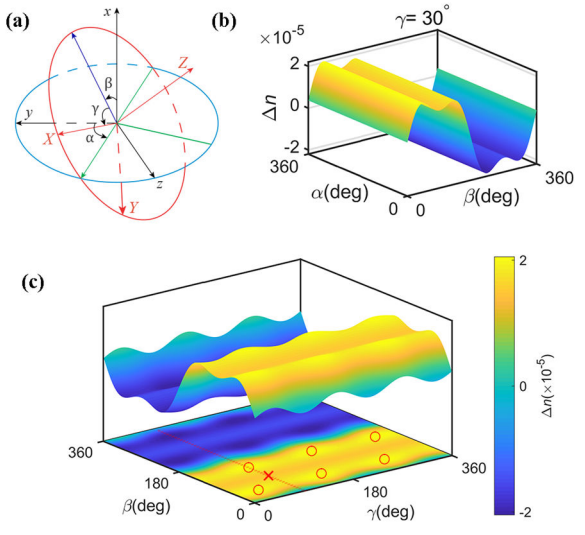

Fig. 2. (a) Schematic of the ordinate system rotation with three steps. (b) Surface plot of calculated refractive index changes Δn with $\gamma = 30°$. (c) Surface plot versus β and γ with its projection below.

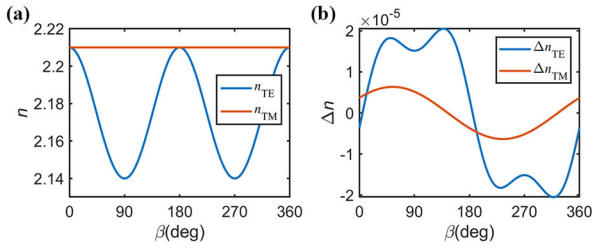

Fig. 3. (a) Calculated refractive indices versus angle β on X-cut TFLN. (b) Calculated refractive index differences versus angle β on X-cut TFLN.

III. NUMERICAL SIMULATION

In a practical TFLN EOM, the driving electric field is more complicated than an ideal uniform field owing to the multi-layer dielectric structure. Moreover, the electric field distribution across the LN waveguides changes with the waveguide directions because of the anisotropic relative permittivity of LN at radio frequency (RF). Therefore, it is necessary to perform numerical simulations for a practical study of the predicted off-axis effect with real field distributions in presence. A finite-element multi-physics-field solver (COMSOL) was used to investigate the angle-dependent efficiencies in three typical TFLN waveguide-electrode configurations, i.e., LN rib waveguide with electrodes on slab [6], Si_3N_4-loaded hybrid waveguide with electrodes on slab [7] and LN rib waveguide with capacitively loaded traveling-wave (CLTW) electrodes on cladding [8]. All parameters are kept identical to the reported studies for each configuration except the waveguide direction to ensure rigorous comparison. The material properties are listed in table I, which are used for simulating optical mode index modulation driven by external RF field applied on the electrodes. The anisotropy is characterized by the permittivity matrix instead of the refractive index matrix in simulations.

With 1-V peak-to-peak driving voltage applied between the electrodes, the field distributions (figs. 4(a-c)) and the effective refractive index change Δn_{eff} (figs. 4(d-f)) versus β (the angle between the waveguide and the crystal axis Z on X-cut TFLN) for the first few modes are obtained and presented. As a result, the simulation results well coincide with the derived theory (fig. 3(d-f)) and present evident efficiency improvement (increased Δn_{eff}) when β deviates from 90°. At $\beta = 90°$, the simulated efficiencies are nearly the same with those in the reported studies (converted from the product of π-shift voltage and length ($V_\pi L$)) with little difference <4%

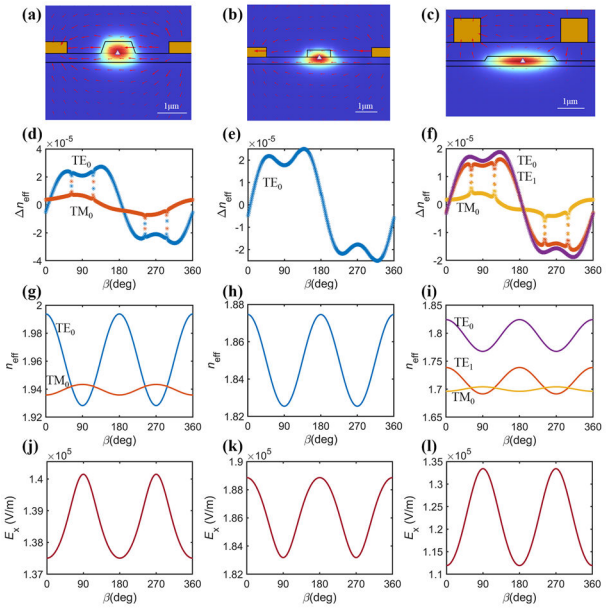

Fig. 4. (a-c) Simulated field distributions of three typical electrode-TFLN waveguide configurations. (d-f) Correponding effective refractive index changes of the first few modes against waveguide direction angle β with external field in presence. (g-i) Corresponding effective refractive indices of the first few modes. (j-l) Corresponding horizontal intensities of the electric field at the triangle-marked positions in (a-c), respectively.

TABLE I. THE MATERIAL PROPERTIES USED IN SIMULATION

Material	Relative permittivity
LN at RF [9]	$\varepsilon_{11} = 42.5, \varepsilon_{33} = 26$
SiO_2 at RF	4
Si at RF	11.9
Si_3N_4 at RF	7.5
Au at RF	1
LN at 1550 nm	$\varepsilon_{11} = 2.21^2, \varepsilon_{33} = 2.14^2$
SiO_2 at 1550 nm	1.444^2
Au at 1550 nm	$(0.52406 + 10.742j)^2$
Si_3N_4 at 1550 nm	1.996^2

(Table II). We also notice that there are discontinuities on the trending curves of Δn_{eff} (figs. 4(d)(f)), which is because of the mode hybridization [10, 11]. The angles corresponding to the discontinuities match with those mode index crossings shown in figs. 4(g) and 4(i). Particularly, when β varies from 90° to 180° with the increasing RF relative permittivity of LN, the trends of the horizonal electric field intensity around the optical mode center (triangle marks in the field distributions) behave oppositely in the LN rib waveguides (figs. 4(j) and 4(l)) and the Si_3N_4-loaded hybrid waveguide (fig. 4(k)). This difference is probably because that Si_3N_4 part has an isotropic relative permittivity but it also subjects to a significant fraction of the electric field.

The main theory and simulation results for TE wave are summarized in Table II for clear comparison. Effective refractive index change induced by external field in conventional Y-propagating waveguide is denoted as $\Delta n_{90°}$. As a consequence, β for the highest efficiencies is between 130° and 140°. We also see that the configuration of electrodes on slab offers the stronger improvement than the CLTW whose electrodes on the cladding. In the cost of less efficiency, the CLTW configurations are preferred to realize better trade-off between optical loss, RF loss, impedance matching and EO velocity matching [12]. However, in the overlapping of the driving electric field and optical mode, a greater vertical component of the electric field could weaken the EO efficiency provided by the horizontal component.

IV. CONCLUSION

In conclusion, theoretical calculation and numerical simulation are performed on EOM with off-axis waveguide

TABLE II. THEORY AND SIMULATION RESULTS

Structure	Reported $\Delta n_{90°}$ ($\times 10^{-5}$)	$\Delta n_{90°}$ ($\times 10^{-5}$)	Δn_{max} ($\times 10^{-5}$)	β at Δn_{max}	Impro-vement
Theory (uniform electric field)	NA	1.514	2.050	138°	35.4%
Electrodes on slab	2.153 [6]	2.088	2.733	135°	30.9%
Si_3N_4 loaded waveguide	1.730 [7]	1.770	2.502	138°	41.4%
CLTW electrodes	1.615 [8]	1.671	2.060	132°	23.3%

orientation on TFLN. The results show that the EO efficiency can be increased by 23% to 42% when the waveguides rotate by certain angles from the conventional Y direction on X-cut TFLN. EOMs on TFLN can be beneficial from this work for efficiency enhancement as well as circuiting flexibility.

ACKNOWLEDGMENT

This work was supported in by the Center-initiated Research Project of Zhejiang Laboratory (K2022ME0AL04), National Key Research and Development Program of China (2021ZD0109904) and Young Scientists Fund of National Natural Science Foundation of China (62105301)

REFERENCES

[1] Y. Qi, and Y. Li, "Integrated lithium niobate photonics," Nanophotonics, vol. 9(6), pp. 1287-1320, 2020.

[2] D. Zhu, L. Shao, M. Yu, R. Cheng, B. Desiatov, C. Xin, Y. Hu, J. Holzgrafe, S. Ghosh, and A. Shams-Ansari, "Integrated photonics on thin-film lithium niobate," Advances in Optics and Photonics, vol. 13(2), pp. 242-352, 2021.

[3] M. Zhang, C. Wang, P. Kharel, D. Zhu, & M. Lončar, "Integrated lithium niobate electro-optic modulators: when performance meets scalability," Optica, vol. 8(5), pp. 652-667, 2021.

[4] R. S. Weis, and T. K. Gaylord, "Lithium niobate: Summary of physical properties and crystal structure," Applied Physics A, vol. 37, pp. 191-203, 1985.

[5] R. W. Boyd, "Nonlinear optics," Academic press, 2020.

[6] C. Wang, M. Zhang, B. Stern, M. Lipson, and M. Lončar, "Nanophotonic lithium niobate electro-optic modulators," Optics express vol. 26(2), pp. 1547-1555, 2018.

[7] P. Zhang, H. Huang, Y. Jiang, X. Han, H. Xiao, A. Frigg, T. G. Nguyen, A. Boes, G. Ren, Y. Su, Y. Tian, and A. Mitchell, "High-speed electro-optic modulator based on silicon nitride loaded lithium niobate on an insulator platform," Optics letters, vol. 46(23), pp. 5986-5989, 2021.

[8] M. Xu, Y. Zhu, F. Pittalà, J. Tang, M. He, W. C. Ng, J. Wang, Z. Ruan, X. Tang, M. Kuschnerov, L. Liu, S. Yu, B. Zhang, and X. Cai, "Dual-polarization thin-film lithium niobate in-phase quadrature modulators for terabit-per-second transmission," Optica, vol. 9(1), pp. 61-62, 2022.

[9] K. K. Wong (Ed.), "Properties of lithium niobate," IET, No. 28, 2002.

[10] J. Wang, P. Chen, D. Dai, and L. Liu, "Polarization Coupling of X -Cut Thin Film Lithium Niobate Based Waveguides," IEEE Photonics Journal, vol. 12(3), pp. 1-10, 2020.

[11] A. Pan, C. Hu, C. Zeng, and J. Xia, "Fundamental mode hybridization in a thin film lithium niobate ridge waveguide," Optics express, vol. 27(24), pp. 35659-35669, 2019.

[12] G. Chen, K. Chen, R. Gan, Z. Ruan, Z. Wang, P. Huang, C. Lu, A. P. T. Lau, D. Dai, C. Guo, and L. Liu, "High performance thin-film lithium niobate modulator on a silicon substrate using periodic capacitively loaded traveling-wave electrode," APL Photonics, vol. 7(2), pp. 026103, 2022